Volume 15
Number 16
21 August 2025
Pages 4601–4886

Catalysis Science & Technology

rsc.li/catalysis

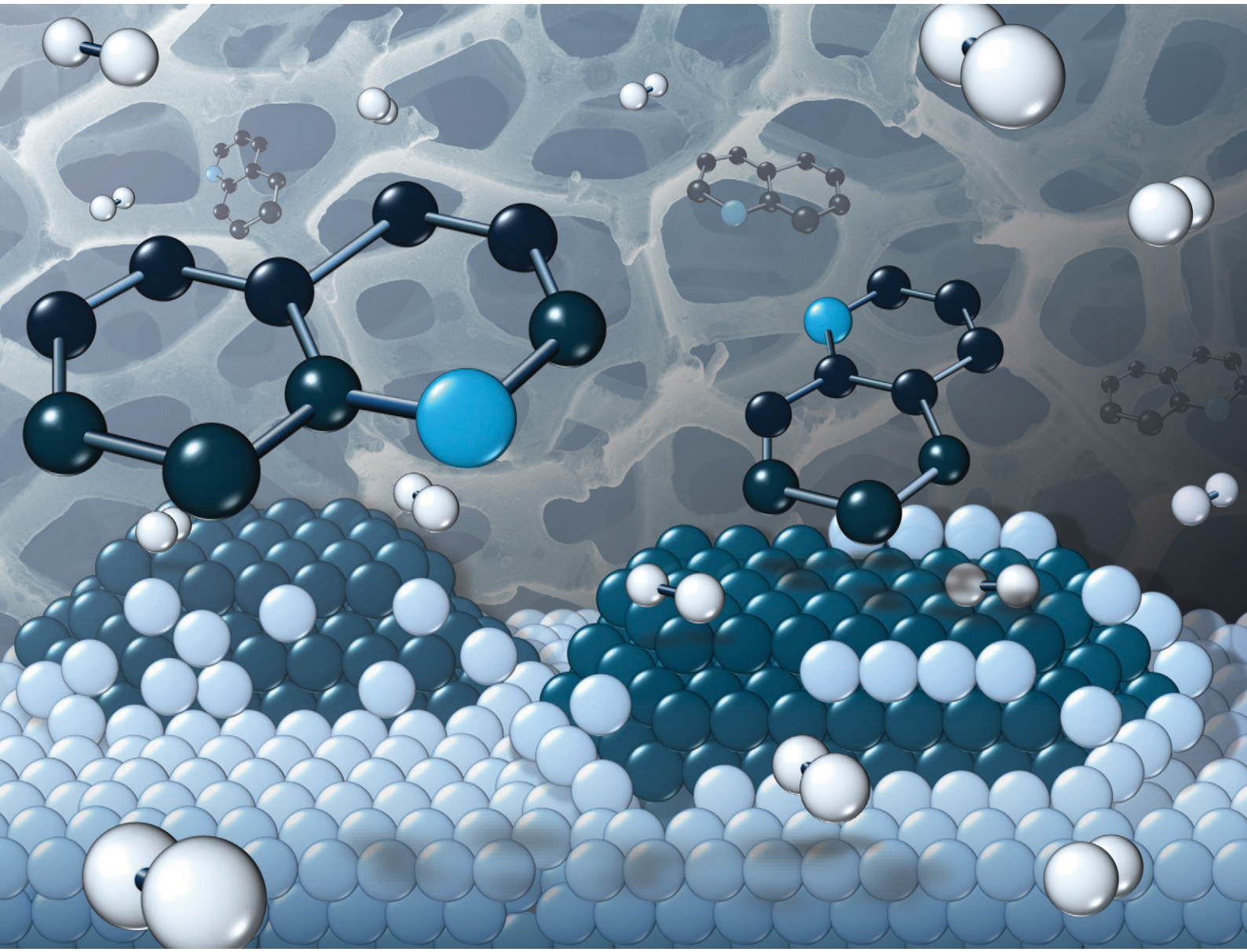

ISSN 2044-4761

ROYAL SOCIETY OF CHEMISTRY

COMMUNICATION
Akihiro Kushima, Titel Jurca *et al.*
Selective and sustainable quinoline hydrogenation with a robust hierarchical catalyst framework

Catalysis Science & Technology

ROYAL SOCIETY OF CHEMISTRY

COMMUNICATION

View Article Online
View Journal | View Issue

Cite this: *Catal. Sci. Technol.*, 2025, **15**, 4632

Received 5th June 2025,
Accepted 2nd July 2025

DOI: 10.1039/d5cy00675a

rsc.li/catalysis

Selective and sustainable quinoline hydrogenation with a robust hierarchical catalyst framework†

Azina Rahmani, [ab] Diego R. Javier-Jiménez, [ab] Deborah Israel,[c] Brian Butkus,[d] Lei Zhai, [ae] Parag Banerjee, [bde] William E. Kaden,[c] Akihiro Kushima [*bd] and Titel Jurca [*abe]

A hierarchical heterogeneous palladium on nickel foam-based catalyst system (Al_2O_3–Pd–D/Ni) was demonstrated for the selective hydrogenation of quinoline and quinoline derivatives under low H_2 pressures, with green solvents (ethanol, ethanol water mixture). The catalyst framework features very low palladium loadings and is highly reusable under facile handling, requiring no filtration or other separation aids, and notably demonstrates no loss in reactivity or alteration of selectivity over multiple recycling trials. Theoretical calculations and X-ray photoelectron spectroscopy studies point to a fully-reduced Pd surface as the necessary active site for catalysis, arising from the *in situ* reduction of the PdO_x surface sites of the air-stable hierarchical material system.

Introduction

Heterogeneous catalytic processes utilizing palladium play a crucial role in a myriad of chemical transformations. While Pd-based catalysts are unequivocally important, there is a need for the sustainable use of palladium due to its increasingly high costs, low natural abundance, high demand across other industries, and concentrated global production.[1–4] Thus, it is imperative to develop robust catalytic systems that can facilitate chemical transformations with low Pd loadings, are amenable to facile reusability, and ideally, operate under sustainable conditions.[5–8]

We have recently described a hierarchical catalyst framework based on nickel foams as contiguous monolith supports.[9] The catalyst relies on bottom-up grown ultralow-loading Pd/PdO_x nanoparticles (0.017% w/w; 15.86 ± 6.85 nm) on a carbonized polydopamine interface, with a subsequent ~2 nm atomic layer deposition (ALD) overcoat of Al_2O_3; Al_2O_3–Pd–D/Ni (Fig. 1A). It was demonstrated that the ultrathin Al_2O_3 overcoat is critical for stabilizing the catalyst framework, and for preferentially blocking low-coordinate sites on the Pd particles which can lead to enhanced selectivity. Al_2O_3–Pd–D/Ni proved to be an exceptionally robust catalyst for the selective hydrogenation of styrene derivatives, nitroaromatics, and anthracene under mild conditions using ethanol as a sustainable solvent (Fig. 1B). Furthermore, owing to the contiguous porous nature of the Ni foam support, Al_2O_3–Pd–D/Ni was directly applicable to flow processes.[9]

The expansion of sustainable and selective heterogeneous hydrogenations to increasingly complex fine chemicals is a topic of intense current interest. N-heterocyclic motifs are ubiquitous across fine chemicals, dyes, and pharmaceuticals.[9–14] Therein,

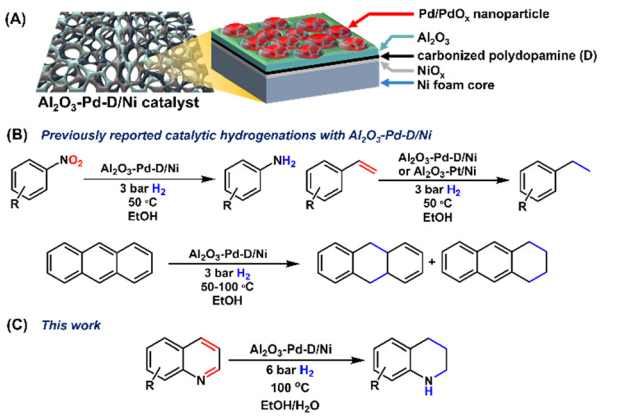

Fig. 1 General schematic for the hierarchical Ni-foam supported Pd catalyst framework (A) previously reported for the catalytic hydrogenation of nitroaromatics, styrenes, and anthracene (B) and the hydrogenation of quinolines (C) reported herein.

[a] *Department of Chemistry, University of Central Florida, Orlando, Florida 32816, USA. E-mail: Titel.Jurca@ucf.edu*
[b] *Renewable Energy and Chemical Transformations Cluster, University of Central Florida, Orlando, Florida, 32816, USA*
[c] *Department of Physics, University of Central Florida, Orlando, Florida 32816, USA*
[d] *Department of Materials Science and Engineering, University of Central Florida, Orlando, Florida, 32816, USA*
[e] *NanoScience Technology Center, University of Central Florida, Orlando, Florida, 32826, USA*

† Electronic supplementary information (ESI) available: Experimental details, ^1H NMR of catalytic experiments, and additional computational details. See DOI: https://doi.org/10.1039/d5cy00675a

the selective hydrogenation of quinolines which can afford 1,2,3,4-tetrahydroquinoline (Py-THQ), 5,6,7,8-tetrahydroquinoline (bz-THQ), or decahydroquinoline (DHQ) has drawn significant attention as both a model catalyst test substrate, and an avenue towards diversified quinoline derivatives.[9–20] These substrates are typically difficult to hydrogenate due to the high resonance stability of the aromatic rings, as well as the potential for catalyst deactivation upon formation of the respective cyclic amines.[11,14,16] Nonetheless, there have been significant contributions towards the utilization of Pd-based quinoline hydrogenation reactions.[11–13,17,20–22] However, these transformations typically require high pressure,[20,22] high temperature,[17] or high catalyst loading.[12,17] Herein, we report the selective hydrogenation of quinoline derivatives utilizing Al_2O_3–Pd–D/Ni, with low Pd loading, low hydrogen pressures, and highly sustainable solvents (EtOH and H_2O).

Results and discussion

Catalytic hydrogenation of quinoline was initially tested using a modified protocol previously established for anthracene;[9] 0.5 mmol quinoline, 5 mL EtOH, ~100 mg piece of Al_2O_3–Pd–D/Ni, 6 bar of H_2, at 100 °C for 18 h (Fig. 2A). Under these conditions, quinoline was quantitatively converted to Py-THQ. To better understand this system, a conversion and selectivity time profile was constructed by performing individual experiments at t = 2, 4, 6, 8, 12, 16 and 24 h (Fig. 2B). Each experiment utilized a different piece of Al_2O_3–Pd–D/Ni catalyst of similar weight (97.75 ± 2.05 mg). It is noteworthy that even with the sample-to-sample inhomogeneity inherent to a monolith-based catalyst, the behavior is remarkably consistent. Under the conditions tested, complete hydrogenation is achieved at 6 hours and the high selectivity towards Py-THQ does not change even at longer reaction times of up to 24 h. Using a gravimetric approach (by mass of Pd), at 2 h we observe 32% conversion, which translates to a competitive turnover frequency (TOF) of *ca.* 500 h^{-1}.[23]

To establish facile reusability, five recycling trials were conducted according to the conditions noted in Fig. 2A, utilizing a 92 mg piece of Al_2O_3–Pd–D/Ni. Across five trials, no change in the quantitative conversion or selectivity towards Py-THQ was observed (Fig. 2C). Unlike conventional nanocatalysts, the isolation of Al_2O_3–Pd–D/Ni requires no filtration aids or centrifugation. The solid piece of Ni foam-based monolith is removed by tweezers, rinsed under flowing deionized water, then EtOH, and allowed to dry overnight under ambient. It can be concluded that Al_2O_3–Pd–D/Ni is remarkably stable under continued use, under refluxing EtOH in a reducing environment, and is physically robust under repeated handling.

We extended the methodology (with 18 h reaction times) to a variety of functionalized derivatives (Fig. 3). The presence of –CH_3 or –OH at the 8 position (**b**, **c**) yielded near quantitative conversion with similar selectivity for hydrogen addition at the 1,2,3,4 positions. Switching to –OCH_3 at the 8 position (**d**) lowered the conversion to 71%, while maintaining high selectivity. Introduction of –Cl at the 6 position (**e**) yielded a lower overall conversion, but maintained high selectivity with no evidence for significant hydrodehalogenation. The presence of –CH_3 groups at the 2 and 4 positions (**f**) did not impede complete conversion, however selectivity for the 1,2,3,4 was observed to be *ca.* 26%, with addition at the 5,6,7,8 being preferred at 74%, likely due to steric factors and the interaction with the catalyst surface; this result is further evaluated by density functional theory (DFT) studies (*vide infra*). In the case of 9-CH_3 acridine (**g**), near quantitative conversion was achieved with 97% selectivity for hydrogenation at the 1,2,3,4 and 5,6,7,8 positions. Attempted hydrogenation of quinoline with an

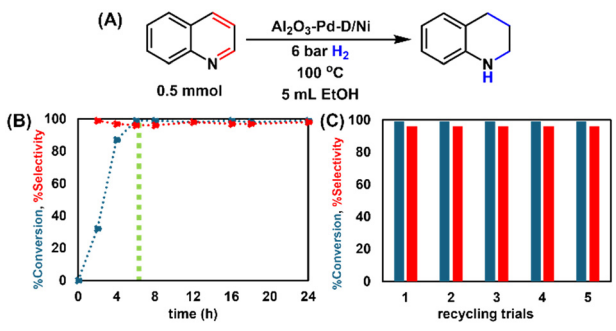

Fig. 2 (A) Reaction scheme for the catalytic hydrogenation of quinoline with Al_2O_3–Pd–D/Ni. (B) Conversion/selectivity *vs.* time utilizing 97.75 ± 2.05 mg of Al_2O_3–Pd–D/Ni (each point = separate reaction); *green dotted line denotes reaction completion at the 6 h timepoint*. (C) Recycling trials, 6 h reaction times, utilizing 92.0 mg of Al_2O_3–Pd–D/Ni.

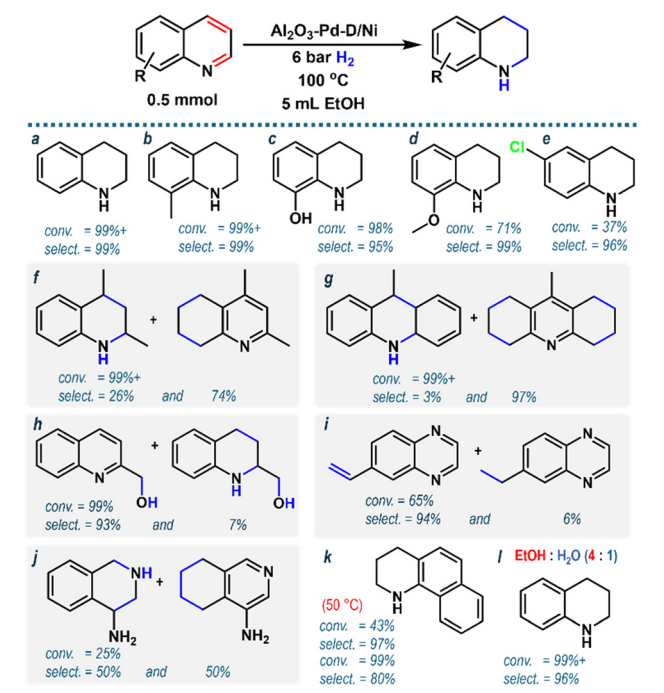

Fig. 3 Scope of catalytic hydrogenation of quinoline derivatives utilizing 95.8 ± 7.4 mg of Al_2O_3–Pd–D/Ni for **a**–**l**. Reaction time = 18 hours.

aldehyde at the 2 position (**h**) yielded complete conversion with preferred selectivity towards the hydrogenation of the aldehyde, and only 7% for both the aldehyde and the 1,2,3,4 of the quinoline. Hydrogenation of quinoxaline functionalized with a terminal alkyne at the 7 position (**i**) resulted in a 65% conversion, favoring the semi-hydrogenation product by 94%; no hydrogens were added to the quinoxaline core. Addition of hydrogen to 4-aminoisoquinoline (**j**) only furnished 25% conversion, with approximately equal preference for the 1,2,3,4 and 5,6,7,8 positions. Hydrogenation of 7,8-benzoquinoline (**k**) yielded complete conversion, with 80% selectivity for hydrogenation at 1,2,3,4. Reduction of temperature to 50 °C lowered the conversion to 43%, with near quantitative selectivity at the 1,2,3,4 position.

To further improve the sustainability of this process, we explored the introduction of H_2O as a reaction co-solvent (Fig. 3. **l**). First, conducting the reaction under similar conditions noted above with a 4 : 1 EtOH:H_2O mixture resulted in complete consumption of the quinoline with near quantitative yield of Py-THQ (**l**). Switching to 100% H_2O as solvent similarly furnished quantitative conversion, but hampered facile isolation and characterization, with the presence of secondary intractable products (Fig. S19†). However, the result validates the potential to run such reactions with "wet" EtOH, *e.g.* bioethanol, which precludes further processing to generate dry solvent, or other efforts to exclude H_2O from the reaction process. Overall, this is promising for enhanced process sustainability.[24]

In our prior work it was surmised that the PdO_x was reduced *in situ* to provide a reactive Pd^0 surface.[9] Herein, to examine the fate of the surface under reaction-like conditions, *in situ* X-ray photoelectron spectroscopy (XPS) was conducted at 100 °C in the presence of H_2. Fig. 4 provides *in situ* Pd 3d XPS spectra collected from the Al_2O_3–Pd–D/Ni interface as a function of sample environment and temperature. The binding energy (BE) scale used to present the Pd 3d XPS data has been adjusted by +0.7 eV to place the primary adventitious C 1s peak at a BE of 284.8 eV.[25] The pristine catalyst exhibits a bimodal peak structure indicative of both PdO (red fits with Pd $3d_{5/2}$ BE = 336.8 eV) and metallic Pd^0 (green fits with Pd $3d_{5/2}$ BE = 335.0 eV).[25] The relative abundance of these species is unaffected by introduction of 1×10^{-3} mBar Ar/H_2 3% at room temperature, but the Pd 3d : Ni 2p XPS peak area ratio attenuates by ~20% indicating subtle attrition of Pd surface site density. Heating to 100 °C within the Ar/H_2 3% environment leads to near complete reduction of PdO to metallic Pd^0 and further loss of Pd surface site concentration *via* some combination of sintering, adlayer formation and/or partial support encapsulation resulting from strong metal–support interactions. Independent of mechanism, the diminished surface site concentration of Pd is present in its fully reduced metallic state when exposed to conditions approximating those described above for the catalytic hydrogenation of quinoline(s).

To better understand the prevailing surface interactions that can be in effect at lower temperatures where PdO_x species dominate, and elevated temperatures where the entire surface is Pd^0 (*vide supra*), DFT simulations were conducted (Fig. 5). The calculations focused on quinoline "Q" where hydrogenation proceeded as expected at the 1,2,3,4 position, and 2,4-dimethylquinoline "Q-2,4", where hydrogen addition at the 5,6,7,8 was significantly preferred. DFT simulations were conducted to calculate the adsorption energies and analyze the atomic structures of the molecules on the surface of both oxidized and reduced Pd surfaces.

First, a lattice constant of Pd was obtained using an FCC unit cell containing four Pd atoms. Post structural optimization, using this lattice constant, a slab model with a Pd(111) surface was constructed, containing 90 Pd atoms and consisting of 3 layers of (111) planes with orthogonal lattice vectors corresponding to [1$\bar{1}$0], [11$\bar{2}$], and [111], with 15 Å of vacuum layer added in [111]. For PdO, two layers of oxygen atoms were added on and below the top Pd surface at cubic PdO sites containing 90 Pd and 60 O atoms. After a Q or Q-2,4 molecule was placed on the surface, molecular dynamics (MD) simulations were conducted (300 K, 1 ps) followed by structural optimization to calculate the molecular adsorption energies using $E_T - (E_s + E_m)$; E_T, E_s, and E_m are calculated potential energies of the molecule-adsorbed surface, surface slab model, and free-standing molecule, respectively. During MD and

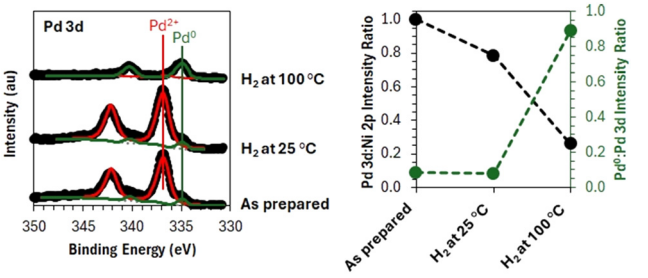

Fig. 4 (Left) *In situ* Pd 3d XPS collected from the as prepared Al_2O_3–Pd–D/Ni interface at 25 °C within UHV (lower), at 25 °C within 1×10^{-3} mBar Ar/H_2 3% (middle), and at 100 °C within 1×10^{-3} mBar Ar/H_2 3% (upper). (Right) Variation in the Pd 3d : Ni 2p (black) and Pd^0 : Pd 3d (green) XPS peak area ratios as a function of sample environment and temperature.

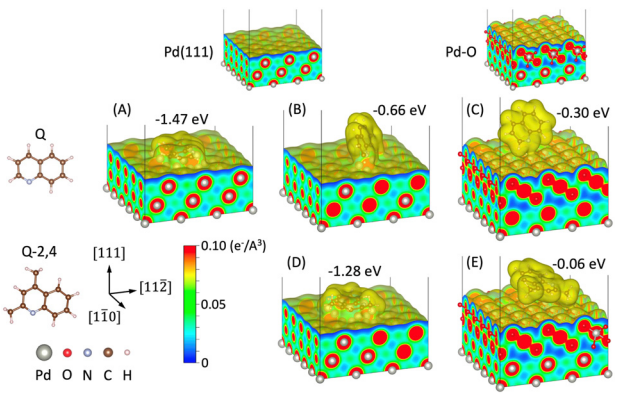

Fig. 5 Adsorption energy and structure of quinoline (Q) on (A and B) Pd(111) and (C) PdO surface and 2,4-dimethylquinoline (Q-2,4) on (D) Pd(111) and (E) PdO surface. Charge density isosurface of 0.005 e^- $Å^{-3}$ is shown.

structural optimization process, the Pd atoms at the bottom layer and the size/shape of the simulation box were fixed. The simulations were performed using Vienna *ab initio* simulation package (VASP).[26,27] A plane-wave energy cut-off of 520 eV was employed, and a generalized gradient approximation parameterized by Perdew, Burke and Ernzerho[28] was used for the exchange-correlation functional. The ionic core was represented with a projector augmented wave potential.[29,30] 11 × 11 × 11 and 2 × 2 × 1 Monkhorst–Pack[31] *k*-point mesh were used for the bulk and the slab models, respectively.

Fig. 5 shows adsorption energy and atomic/electronic structure of the Pd(111) and PdO surface with Q and 2,4-Q molecules. Two different configurations were obtained for Q on Pd(111) surface depending on the initial structures. The molecule lying flat on the surface has a higher adsorption energy at −1.47 eV compared with the tilted configuration at −0.66 eV. The adsorption energy of 2,4-Q on Pd(111) was −1.28 eV. On the other hand, the values for Q and 2,4-Q on PdO were −0.30 eV and −0.06 eV, respectively. Both molecules favor the reduced Pd surface. This is consistent with the literature which points to a preferential flat configuration on Pd^0 (*e.g.* Pd(111)) sites.[32–34] This can be also seen from the charge density distributions. Electrons are conforming the molecules on the bare Pd(111) surface, while they are bound only at the edge of the molecules as shown in (C) and (E). Differential charge density distributions were compared to analyze the bonding between the molecule and the surface in more detail (Fig. S20†). The result confirms that the molecular adsorption on bare Pd surface was chemisorption, while it was physisorption on PdO, which agrees well with the difference in the adsorption energies. Here, the rearrangement of electrons for chemisorbed molecules were localized at the binding atoms for tilted configurations. Hahn and Baiker report similar chemisorption and flat Q orientation with Pd^0 while in their case, tilted Q configuration and physisorption with an Au^0 surface.[34] This change in the electronic structure contributes to accelerating the catalytic reaction of the molecules on the bare Pd, which is consistent with our experimental measurement. Although the flat configuration is more energetically favorable, other molecules adsorbed on the surface such as H_2/C_2H_5OH or surface roughness may prevent the molecules from lying flat. In addition, a partially oxidized surface is expected to promote tilted adsorption, and the chemical bond between the adsorbed molecule and Pd atoms enhances the catalytic reactions. However, a fully oxidized Pd surface hinders activity as only physisorption is allowed.

Thus, a reduced Pd^0 surface of sufficient dimension to facilitate chemisorption and subsequent reactivity with surface-bound H_2 is required and falls in line with experimental observations from both catalysis and *in situ* XPS (*vide supra*). The presence of steric bulk and other functional groups impede both the initial physisorption on PdO, and lead to lower energy interactions on Pd^0, and in the case of 2,4-Q lead to preferential hydrogenation on the phenyl portion of the quinoline framework, which is directly interfacing with the surface.

Conclusions

Hierarchical nickel foam-based Al_2O_3–Pd–D/Ni was demonstrated as an excellent catalyst framework for the selective hydrogenation of quinoline derivatives utilizing low H_2 pressures and green solvents (EtOH and H_2O), and leveraging an inherently low Pd loading. The selectivity observed towards 1,2,3,4-tetrahydroquinoline may prove advantageous compared to very common Pd-based hydrogenation catalysts, such as Pd/C which has been shown to fully hydrogenate quinoline to decahydroquinoline even under very mild conditions (room temperature and H_2 balloon).[35] The catalyst framework is highly reusable under facile handling, requiring no filtration media or other separation aids, and notably demonstrates no loss in reactivity or alteration of selectivity over multiple trials. Thus, while the catalyst system uses Pd, the extremely low loading, and high degree of reusability drastically enhance it's sustainability.

Data availability

All relevant information is provided in the ESI.† Further information and/or clarification can be provided by the authors upon request.

Conflicts of interest

There are no conflicts to declare.

Acknowledgements

This work was supported by the Departments of Chemistry and Physics (College of Sciences), the Department of Materials Science and Engineering (College of Engineering and Computer Science) and the Faculty Cluster Initiative at the University of Central Florida. The authors thank the PREM Center for Quantum Materials Innovation and Education Excellence funded by the National Science Foundation (NSF) with Award No. 2424976. *In situ* XPS analysis was completed within the University of Central Florida's Materials Characterization Facility using equipment procured using NSF Grant No. 2018319.

Notes and references

1 C. Torborg and M. Beller, *Adv. Synth. Catal.*, 2009, **351**, 3027–3043.
2 L. B. Vitaliy, S. S. Peter, H. C. James and L. Rafael, *Curr. Org. Synth.*, 2010, **7**, 614–627.
3 P. Devendar, R. Y. Qu, W. M. Kang, B. He and G. F. Yang, *J. Agric. Food Chem.*, 2018, **66**, 8914–8934.
4 S. Xu, E. H. Kim, A. Wei and E. Negishi, *Sci. Technol. Adv. Mater.*, 2014, **15**, 044201.
5 S. McCarthy, D. C. Braddock and J. D. E. T. Wilton-Ely, *Coord. Chem. Rev.*, 2021, **442**, 213925.
6 S. Mitchell, E. Vorobyeva and J. Pérez-Ramírez, *Angew. Chem., Int. Ed.*, 2018, **57**, 15316–15329.

7 J. Liu, *ACS Catal.*, 2017, **7**, 34–59.
8 L. R. Shultz-Johnson, A. Rahmani, J. Frisch, T. E. Hsieh, L. Hu, J. Sosa, M. Davy, S. Xie, M. J. Beazley, Z. Gao, P. Golvari, T. H. Wang, T. G. Ong, N. G. Rudawski, F. Liu, P. Banerjee, X. Feng, M. Bär and T. Jurca, *ACS Appl. Mater. Interfaces*, 2024, **16**, 39387–39398.
9 A. Rahmani, T. M. Currie, L. R. Shultz, J. T. Bryant, M. J. Beazley, F. J. Uribe-Romo, L. Tetard, N. G. Rudawski, S. Xie, F. Liu, T. H. Wang, T. G. Ong, L. Zhai and T. Jurca, *Catal. Sci. Technol.*, 2022, **12**, 6992–6997.
10 Y. Hu, M. Liu, S. Bartling, H. Lund, H. Atia, P. J. Dyson, M. Beller and R. V. Jagadeesh, *Sci. Adv.*, 2023, **48**, eadj8225.
11 M. M. Dell'Anna, V. F. Capodiferro, M. Mali, D. Manno, P. Cotugno, A. Monopoli and P. Mastrorilli, *Appl. Catal., A*, 2014, **481**, 89–95.
12 Y. Zhang, J. Zhu, Y. T. Xia, X. T. Sun and L. Wu, *Adv. Synth. Catal.*, 2016, **358**, 3039–3045.
13 X. Ding, Y. Chen, J. Nan, H. Dai, Y. Wang, G. Bai and W. Qiu, *ACS Sustainable Chem. Eng.*, 2022, **10**, 14011–14023.
14 F. Chen, A. E. Surkus, L. He, M. M. Pohl, J. Radnik, C. Topf, K. Junge and M. Beller, *J. Am. Chem. Soc.*, 2015, **137**, 11718–11724.
15 L. Bai, X. Wang, Q. Chen, Y. Ye, H. Zheng, J. Guo, Y. Yin and C. Gao, *Angew. Chem., Int. Ed.*, 2016, **55**, 15656–15661.
16 H. Cho, F. Török and B. Török, *Org. Biomol. Chem.*, 2013, **11**, 1209–1215.
17 A. Mollar-Cuni, S. Martín, G. Guisado-Barrios and J. A. Mata, *Carbon*, 2023, **206**, 314–324.
18 M. N. Shaikh, *RSC Adv.*, 2019, **9**, 28199–28206.
19 S. Li, Y. Yang, Y. Wang, H. Liu, J. Tai, J. Zhang and B. Han, *Catal. Sci. Technol.*, 2018, **8**, 4314–4317.
20 S. Zhang, Z. Xia, T. Ni, H. Zhang, C. Wu and Y. Qu, *J. Mater. Chem. A*, 2017, **5**, 3260–3266.
21 M. Guo, C. Li and Q. Yang, *Catal. Sci. Technol.*, 2017, **7**, 2221.
22 Y. Ren, Y. Wang, X. Li, Z. Zhang and Q. Chi, *New J. Chem.*, 2018, **42**, 16694.
23 D. Chandra, S. Saini, S. Bhattacharya, A. Bhaumik, K. Kamata and M. Hara, *ACS Appl. Mater. Interfaces*, 2020, **12**, 52668–52677.
24 D. Prat, A. Wells, J. Hayler, H. Sneddon, C. R. McElroy, S. Abou-Shehada and P. J. Dunn, *Green Chem.*, 2016, **18**, 288–296.
25 J. F. Moulder, W. F. Stickle, P. E. Sobol and K. D. Bomben, in *Handbook of X-ray Photoelectron Spectroscopy*, ed. J. Chastain, Perkin-Elmer Corporation Physical Electronics Division, Minnesota, 1992.
26 G. Kresse and J. Hafner, *Phys. Rev. B*, 1993, **47**, 558.
27 G. Kresse and J. Furthmüller, *Phys. Rev. B*, 1996, **54**, 11169.
28 J. P. Perdew, K. Burke and M. Ernzerhof, *Phys. Rev. Lett.*, 1996, **77**, 3865.
29 G. Kresse and D. Joubert, *Phys. Rev. B*, 1999, **59**, 1758.
30 P. E. Blöchl, *Phys. Rev. B*, 1994, **50**, 17953.
31 H. J. Monkhorst and J. D. Pack, *Phys. Rev. B*, 1976, **13**, 5188.
32 J. M. Bonello, R. Lindsay, A. K. Santra and R. M. Lambert, *J. Phys. Chem. B*, 2002, **106**, 2672.
33 G. Santarossa, M. Iannuzzi, A. Vargas and A. Baiker, *ChemPhysChem*, 2008, **9**, 401.
34 K. R. Hahn and A. Baiker, *J. Phys. Chem. C*, 2022, **126**, 20840.
35 N. Tanaka and T. Usuki, *Eur. J. Org. Chem.*, 2020, 5514.

